Analysis of Local Quasi-Stationarity Regions in an Urban Macrocell Scenario

Adrian Ispas and Gerd Ascheid
Institute for Integrated Signal Processing Systems
RWTH Aachen University, Germany
{ispas, ascheid}@iss.rwth-aachen.de

Christian Schneider and Reiner Thomä
Institute of Information Technology
Ilmenau University of Technology, Germany
{christian.schneider, reiner.thomae}@tu-ilmenau.de

***Abstract*—A common simplification in the treatment of random linear channels is the wide-sense stationary and uncorrelated scattering (WSSUS) assumption. For wireless channels, this assumption is, however, only fulfilled in an approximative sense inside local time-frequency regions. Since algorithms in wireless digital communications often rely on knowledge of second order statistics of the channel, it is important to know the size of local quasi-stationarity regions. Thus, we determine quasi-stationarity regions in distance for an urban macrocell scenario. We observe that, based on the chosen measure and in our specific scenario, the time-frequency properties are dominant compared to the spatial properties in defining the size of quasi-stationarity regions. Furthermore, we find that in some cases the quasi-stationarity regions strongly depend on the mobile terminal orientation.**

I. Introduction

Common simplifications in the treatment of random linear channels are the wide-sense stationary (WSS) and the uncorrelated scattering (US) assumption. Together these two properties define a WSSUS channel. However, early empirical evidence for non-WSSUS wireless single-input and single-output (SISO) channels, i.e., non-stationary wireless SISO channels in time and frequency, can be found in, e.g., [1] for an indoor channel and in [2] for an outdoor channel. Therefore, the determination of quasi-stationarity regions, i.e., regions in which a stochastic process is approximated as stationary, is important for algorithms which rely on knowledge of, e.g., second order statistics of the channel.

In [3], the quasi-WSSUS SISO channel model is introduced. This model separates the randomness of the channel in a fast and a slow fading part to define local WSSUS channels. In [4], a framework for non-WSSUS SISO channels, which are doubly underspread (DU), i.e., in dispersion and correlation, is introduced. The concept of a scattering function is extended to non-stationary random processes and named (generalized) local scattering function ((G)LSF). For DU channels an estimator of the GLSF is presented in [5] and [6].

In order to determine quasi-stationarity regions, appropriate measures are needed. For a SISO channel these can be based on the GLSF: one measure is the collinearity [6], which is a normalized variant of the standard inner product in Euclidean space. Another measure, called the spectral divergence [7], was originally introduced to compare power spectral densities. For a multiple-input and multiple-output (MIMO) channel, in [8] and [9], a measure called the correlation matrix distance (CMD) is used. It does not consider the time-frequency properties, but characterizes only the (dis)similarity of the spatial properties between two correlation matrices. This is especially useful for spatially based algorithms.

Contribution: The goal of this paper is to determine quasi-stationarity regions in distance for the wireless channel in an urban macrocell scenario. In particular, based on the collinearity measure, we

- study the dependence of these quasi-stationarity regions on the orientation of the mobile terminal (MT) antennas,
- compare the quasi-stationarity of the time-frequency and the spatial properties for our specific scenario,
- analyze the quasi-stationarity of the spatial properties at the MT and the base station (BS), individually and jointly.

We emphasize that we only study quasi-stationarity in distance and of second order moments only.

Notation: $\mathrm{F}_{t\to f}\{\cdot\}$ denotes the Fourier transform from the t to the f domain, and $\mathrm{F}^{-1}_{f\to t}\{\cdot\}$ its inverse. $(x *_n y)(\cdot)$ denotes the n-dimensional convolution of $x(\cdot)$ and $y(\cdot)$. $|\mathcal{A}|$ denotes the cardinality of the set $\mathcal{A}$. $\mathrm{tr}\{\mathbf{A}\}$ and $||\mathbf{A}||_F$ denote the trace and the Frobenius norm of the matrix $\mathbf{A}$, respectively. $\mathbf{A}\oplus\mathbf{B}$ denotes the block matrix resulting from the direct sum of the matrices $\mathbf{A}$ and $\mathbf{B}$.

II. Local Scattering Function

The local scattering function (LSF) is an extension of the scattering function in the context of WSSUS channels to the non-stationary case. It is, thus, a time and frequency dependent power density spectrum in the delay and Doppler domain. It is defined according to

$$C_{\mathrm{H}}(t,f;\nu,\tau) \triangleq \mathrm{F}_{\Delta t\to\nu}\left\{\mathrm{F}^{-1}_{\Delta f\to\tau}\left\{R_{\mathrm{H}}(t,f;\Delta t,\Delta f)\right\}\right\} \quad (1)$$

where

$$R_{\mathrm{H}}(t,f;\Delta t,\Delta f) \triangleq \mathrm{E}\left\{L_{\mathrm{H}}(t,f+\Delta f)L^{*}_{\mathrm{H}}(t-\Delta t,f)\right\} \quad (2)$$

is the correlation function and $L_{\mathrm{H}}(t,f)$ denotes the time-varying transfer function of the channel. A second order stationary channel in time and frequency has a constant LSF over t and f, respectively. Note that an up to second order stationary process in time and frequency is uncorrelated in Doppler and delay, respectively. The reverse is only true for a constant, e.g., zero-mean, process. For the rest of the present work, by stationarity, we mean quasi-stationarity of second order moments only, unless otherwise stated.

In [4], the class of DU channels is introduced. These channels are, on the one hand, *dispersion* underspread with a

This work was supported by the Ultra high-speed Mobile Information and Communication (UMIC) research centre and the Network of Excellence in Wireless COMmunications NEWCOM++.

maximal delay-Doppler product $\tau_{max}\nu_{max} \ll 1$. This property is well known from WSSUS channels. On the other hand, they are *correlation* underspread with $\frac{\Delta\tau_{max}\Delta\nu_{max}}{\tau_{max}\nu_{max}} \ll 1$, where $\Delta\tau_{max}$ and $\Delta\nu_{max}$ denote the maximal correlation in delay and Doppler, respectively. This essentially means that the time-frequency coherence region is much smaller than the corresponding stationarity region.

The LSF has some deficiencies, e.g., it is not guaranteed to be positive. For DU channels it is possible to define generalized local scattering functions (GLSFs) [4]

$$C_{\mathrm{H}}^{(\Phi)}(t,f;\nu,\tau) \triangleq (C_{\mathrm{H}} *_4 \Phi)(t,f;\nu,\tau) \tag{3}$$

with

$$\begin{aligned}\Phi(t,f;\nu,\tau) = \sum_{k=1}^{K}\gamma_k \int_{-\infty}^{\infty}\int_{-\infty}^{\infty} L_{\mathrm{G}_k}^{*}(-t,-f+\Delta f) \\ \times L_{\mathrm{G}_k}(-t-\Delta t,-f) e^{-j2\pi(\nu\Delta t-\tau\Delta f)}\,\mathrm{d}\,\Delta t\,\mathrm{d}\,\Delta f\end{aligned} \tag{4}$$

where $L_{\mathrm{G}_k}(t,f)$ are windowing functions in time-frequency, $\gamma_k \geq 0$ normalizing constants, and K the number of windows used. From this, it can be seen that a GLSF is a smoothed version of the LSF. The GLSFs have practically important properties: they are real-valued and positive, and, for DU channels, approximately equivalent. For further details we refer to [4]. Neither the LSF, nor the GLSF is directly obtainable from measurements. However, for DU channels an estimation of the GLSF, i.e., a spectral estimator, using only a single measurement per track is proposed in [5] and [10].

Since the channel measurements are available at discrete time and frequency instants, we are interested in a discrete representation of the GLSF. One obtains in this case [6]

$$C_{\mathrm{H}}^{(\Phi)}[m,q;p,n] = \sum_{k=0}^{K-1}\gamma_k \,\mathrm{E}\left\{\left|H^{G_k}[m,q;p,n]\right|^2\right\} \tag{5}$$

with

$$\begin{aligned}H^{\mathrm{G}_k}[m,q;p,n] \;=\; \sqrt{T_s F_s}\sum_{m'=-\lfloor N_t/2\rfloor}^{\lceil N_t/2\rceil-1}\;\sum_{q'=-\lfloor N_f/2\rfloor}^{\lceil N_f/2\rceil-1} L_{\mathrm{G}_k}^{*}[m',q'] \\ \times\; L_{\mathrm{H}}[m+m',q+q'] e^{-j2\pi\left(\frac{pm'}{N_t}-\frac{nq'}{N_f}\right)}.\end{aligned} \tag{6}$$

$L_{\mathrm{H}}[m,q]$, $L_{\mathrm{G}_k}[m,q]$, m, q, p, and n are the discrete equivalents to the continuous case. N_t and N_f denote the window lengths in time and frequency, respectively. T_s and F_s are the time and frequency difference between consecutive samples, respectively. By removing the expectation operator in (5), we obtain the GLSF estimator from [5] in the discrete setting.

III. Measures for Stationarity Regions

In order to obtain stationarity regions, we need appropriate measures that can be compared to chosen thresholds. When studying stationarity in time of the time-frequency properties only, we use the collinearity of the GLSF between different time instances for all MIMO sublinks:

$$\begin{aligned}col_{\mathbf{C}_{\mathrm{H}}^{(\Phi)}}[m,m'] &\triangleq \mathrm{col}\left\{\mathbf{C}_{\mathrm{H}}^{(\Phi)}[m,q],\mathbf{C}_{\mathrm{H}}^{(\Phi)}[m',q]\right\} \\ &\triangleq \frac{\mathrm{tr}\left\{\mathbf{C}_{\mathrm{H}}^{(\Phi)\,H}[m,q]\mathbf{C}_{\mathrm{H}}^{(\Phi)}[m',q]\right\}}{\left\|\mathbf{C}_{\mathrm{H}}^{(\Phi)}[m,q]\right\|_F\left\|\mathbf{C}_{\mathrm{H}}^{(\Phi)}[m',q]\right\|_F}\end{aligned} \tag{7}$$

with the block matrix

$$\mathbf{C}_{\mathrm{H}}^{(\Phi)}[m,q] \triangleq \mathbf{C}_{\mathrm{H},sl=1}^{(\Phi)}[m,q]\oplus\ldots\oplus\mathbf{C}_{\mathrm{H},sl=N_{TX}N_{RX}}^{(\Phi)}[m,q] \tag{8}$$

and $[\mathbf{C}_{\mathrm{H},sl=i}^{(\Phi)}[m,q]]_{p,n} \triangleq C_{\mathrm{H}}^{(\Phi)}[m,q;p,n]$ for the MIMO sublink i. N_{TX} and N_{RX} denote the number of antennas considered in the MIMO link on transmitter (TX) and receiver (RX) side, respectively. Furthermore, $\mathrm{col}\{\mathbf{X},\mathbf{Y}\} \in [0,1]$ for $[\mathbf{X}]_{i,j} \geq 0$ and $[\mathbf{Y}]_{i,j} \geq 0$, or for positive semidefinite matrices $\mathbf{X}$ and $\mathbf{Y}$. Here and subsequently, we omit the frequency dependency of the measures, since we do our analysis for a fixed frequency. In a MIMO scenario the GLSF becomes more complex, since the spatial domains at the TX and the RX are added. Therefore, in [8] and [9], the CMD has been proposed. Essentially, the CMD in time characterizes the (dis)similarity in time of the spatial properties of the channel only:

$$\begin{aligned}CMD_i[m,m'] &\triangleq 1-\mathrm{col}\left\{\mathbf{R}_i[m,q],\mathbf{R}_i[m',q]\right\} \\ &= 1-\frac{\mathrm{tr}\left\{\mathbf{R}_i[m,q]\mathbf{R}_i[m',q]\right\}}{\left\|\mathbf{R}_i[m,q]\right\|_F\left\|\mathbf{R}_i[m',q]\right\|_F}\end{aligned} \tag{9}$$

where the (Hermitian and positive semidefinite) matrix R_i can be the full, the TX, or the RX correlation matrix defined as

$$\begin{aligned}\mathbf{R}_{full}[m,q] &= \mathrm{E}\left\{\mathrm{vec}\left\{\mathbf{L}_{\mathrm{H}}[m,q]\right\}\mathrm{vec}\left\{\mathbf{L}_{\mathrm{H}}[m,q]\right\}^H\right\} \\ \mathbf{R}_{TX}[m,q] &= \mathrm{E}\left\{\mathbf{L}_{\mathrm{H}}^{T}[m,q]\mathbf{L}_{\mathrm{H}}^{*}[m,q]\right\} \\ \mathbf{R}_{RX}[m,q] &= \mathrm{E}\left\{\mathbf{L}_{\mathrm{H}}[m,q]\mathbf{L}_{\mathrm{H}}^{H}[m,q]\right\}\end{aligned} \tag{10}$$

with $\left[\mathbf{L}_{\mathrm{H}}[m,q]\right]_{j,i} \triangleq L_{\mathrm{H}}[m,q]$ for the RX element j and the TX element i. Therefore, with (10), one can choose between analyzing the spatial properties at the TX and the RX jointly, the TX only, or the RX only, respectively. We do not use the spectral divergence as in [7], since the collinearity and the CMD are essentially the same measure and, thus, comparable. Furthermore, comparing (7) and (9), one sees that the inclusion of the different sublinks in (7) ensures that the collinearity of the GLSF and the full CMD have the same structure: both measures perform a summation over all MIMO sublinks. Note also that only stationarity of second order moments is characterized by these measures.

Defining sets $\mathcal{M}_j[m]$ using thresholds th_j as

$$\mathcal{M}_{col}[m] \triangleq \left\{m' \mid col_{\mathbf{C}_{\mathrm{H}}^{(\Phi)}}[m,m'] > th_{col}\right\} \tag{11}$$

$$\mathcal{M}_{CMD,i}[m] \triangleq \left\{m' \mid CMD_i[m,m'] < th_{CMD,i}\right\} \tag{12}$$

we obtain time dependent stationarity times

$$T_{stat,j}[m] \triangleq |\mathcal{C}_j[m]|\; T_s \tag{13}$$

where $\mathcal{C}_j[m]$ is the connected subset of $\mathcal{M}_j[m]$ with maximum cardinality and containing m. Generally, thresholds and, thus, the stationarity times depend on the accuracy that is required for the considered algorithm.

IV. MIMO Channel Measurement Campaign

Our MIMO channel measurement campaign focuses on gathering realistic channel data in an urban macrocell scenario in the 3GPP Long Term Evolution (LTE) band. Channel sounding is conducted at 2.53 GHz in 2 bands of 40 MHz.

On the BS side a uniform linear array (ULA) with 8 dual-polarized (horizontally and vertically) elements is used. Each element consists of a stack of 4 patches in order to form a

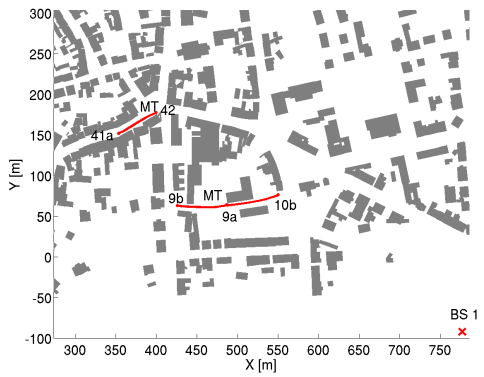

Fig. 1. Overview of the MT reference tracks and the position of BS 1

narrow transmit beam in elevation. At the MT (passenger car) a uniform circular array (UCA) with 2 rings of 12 dual-polarized patches is used. Additionally, a cube with 5 patches is placed on top. The BS serves as the TX and the MT as the RX.

The measurement campaign sequentially covers 3 BS positions with 25 m, 15 m, and 3.5 m height, and a centrally located relay point with 3.5 m height. In total 22 individual tracks with more than 120 measurement runs are performed. In Fig. 1, an overview of the MT reference tracks and BS 1 is shown. Track 10b-9a and 9a-9b feature an increasing distance to BS 1, while track 41a-42 has a rather constant distance.

Table I summarizes the properties of the measurement campaign. For further details we refer to [11] and [12].

GENERAL PROPERTIES		
Scenario	Urban macrocell	
Location	City center, Ilmenau, Germany	
MIMO Measurement setup	3 BSs, 1 relay station, 22 tracks	
Intersite distances	BS 1-2: 680 m, BS 2-3: 580 m, BS 3-1: 640 m	
CHANNEL SOUNDER PROPERTIES		
Type	RUSK TUI-FAU, Medav GmbH	
TX power	46 dBm at the power amplifier output	
Center frequency f_c	2.53 GHz	
Bandwidth	2 bands of 40 MHz	
Time sample spacing T_s	13.1 ms	
Frequency sample spacing F_s	156.25 kHz	
MIMO sublinks	928 ($N_{TX} = 16$, $N_{RX} = 58$)	
AGC switching	In MIMO sublinks	
Positioning	Odometer and GPS	
ANTENNA PROPERTIES		
	TX array	RX array
Type	PULPA8	SPUCPA 2x12 + cube
Height	25 m, 15 m, 3.5 m	1.9 m
Beamwidth, azimuth (3dB)	100°	360°
Beamwidth, elevation (3dB)	24°	80°
Tilt	5° down	0
Maximal velocity $\lvert v_{max}\rvert$	0	$\approx$ 10 km/h

TABLE I
PROPERTIES OF THE MEASUREMENT CAMPAIGN

V. Processing of the Measurement Data

In this work, we choose BS 1 at a height of 25 m as the TX array, the lower UCA at the MT as the RX array, and the 3 reference tracks for our studies. We use the central 20 MHz band in the lower frequency domain of the measurements and study vertically polarized propagation. The considered MIMO link consists of the central 4 antenna elements at the BS (TX) and 3 neighboring antenna elements at the MT (RX) for each orientation at the MT. The 4 orientations are the front (direction of motion), the back, and the 2 sides of the MT. We preprocess the data by estimating a noise level in the time-delay domain and not considering any values below it.

Before performing the GLSF estimation, we verify that the DU assumption holds. For this, we need estimates of the stationarity regions, thus, we can only perform a rough check. The maximal velocity of the MT is $|v_{max}| \approx 10$ km/h. Since the base station is fixed and we assume the scatterers to be fixed for now, we obtain a maximal Doppler frequency $|\nu_{max}| = |v_{max}| f_c / c_0 \approx 23.4$ Hz, with the center frequency f_c and the speed of light in vacuum c_0. This results in a minimal coherence time $T_{c,min} \triangleq 1/|\nu_{max}| = 42.7$ ms. We observe a maximal delay $\tau_{max} \approx 5$ μs, which gives a minimal coherence frequency $F_{c,min} \triangleq 1/\tau_{max} = 200$ kHz. Assuming a minimal stationarity length of $d_{s,min} \approx 10\lambda_c = 10 c_0 / f_c = 1.19$ m [13], a rough estimate of the minimal stationarity time is $T_{s,min} \triangleq 1/\Delta\nu_{max} = d_{s,min}/v_{max} \approx 0.43$ s. We estimate the minimal stationarity in frequency as in [4] assuming that correlation of different delay components is only a result of scattering from the same physical object. Assuming the maximal size of an object to be $w_{max} \approx 15$ m, the minimal stationarity in frequency is $F_{s,min} \triangleq 1/\Delta\tau_{max} \approx c_0/w_{max} \approx 20$ MHz. We, thus, obtain $\Delta\tau_{max}\Delta\nu_{max} \approx 1.16 \cdot 10^{-7}$ and $\tau_{max}\nu_{max} \approx 1.17 \cdot 10^{-4}$ and, thus, the DU assumption $\Delta\tau_{max}\Delta\nu_{max} \ll \tau_{max}\nu_{max} \ll 1$ is fulfilled in our scenario. With the above estimates the minimum number of coherent samples is 3 in time and 1 in frequency. The minimum number of stationary samples is 32 in time and 128 in frequency.

For the windows in the GLSF estimation, we use a separation into time and frequency windows, i.e., $L_{G_{(i-1)I+j}}[m,q] = u_i[m]v_j[q]$, with $i = 1..I$, $j = 1..J$, and $K = IJ = 1/\gamma_k$. Each window is created by a discrete prolate spheroidal sequence (DPSS) [14] as proposed in [5] and [6]. The chosen time-limited DPSSs have unit energy and are optimally concentrated in bandwidth, and, thus, a good choice for a small mean-squared error (MSE) in a DU scenario, as can be concluded from the bias-variance analysis in [5]. For the window lengths in time and frequency we use $N_t = 16$ and $N_f = 128$, respectively. We choose all the values inside the minimal frequency stationarity region to obtain a maximal amount of realizations. In time we use half of the corresponding values, i.e., average over approx. $5\lambda_c$, so as not to risk smoothing out the non-stationary properties in time, but not to lose too much Doppler resolution (here 5.09 Hz), either. The number of windows is set to $I = J = 2$ to limit computational complexity. No claims of optimality are made for the window parameters. For each orientation we include the 3 neighboring antenna elements at the RX in the collinearity of the GLSF, but only include one antenna element at the TX

(when looking at the MT from the BS, number 4 of the 8-element ULA from right), cf. (7). This reduces computational complexity and is feasible, since we expect the patterns of the inner ULA antenna elements at the TX to be similar.

To obtain the CMDs, we need estimates of the correlation matrices. We approximate the ensemble averaging by an averaging operation as is usually done [8]. We average in time over $N_t = 16$ and in frequency over $N_f = 128$ samples for each CMD type. In total we, thus, average over 2048 (≈ 500 non-coherent) realizations. This should be sufficient for an accurate estimation of all CMDs. Note that the TX CMD and RX CMD perform an averaging of the instantaneous correlation matrices over the RX and the TX array, respectively. Our RX array with directional antennas is non-stationary in its spatial domain, and, therefore, averaging can only be interpreted as an ensemble averaging in an approximative sense.

A difficult task is the choice of a threshold, as it depends on the accuracy that is required for the considered algorithm. For the collinearity of the GLSF, we define $th_{col} = 0.9$ as in [6]. Accordingly, for the CMDs we get $th_{CMD,i} = 1 - th_{col} = 0.1$.

VI. Results of the Data Analysis

The results on the stationarity in time are mapped to the driven distance using the positioning information obtained during the measurement campaign. Assuming that only the MT is moving, i.e., scatterers and the BS are fixed, this gives a representation of the stationarity in distance at the MT.

Concerning the analysis of the stationarity in distance of the time-frequency properties only, we exemplarily show the collinearity of the GLSF in Fig. 2 and the corresponding stationarity distances in Fig. 3 per orientation for track 9a-9b. The front and the right orientation have a similar structure with a peak in the stationarity distances at the beginning of the track. There the MT moves into an open area. The back and the left orientation have a similar structure as well, but with a peak in the stationarity distances in the middle of the track,

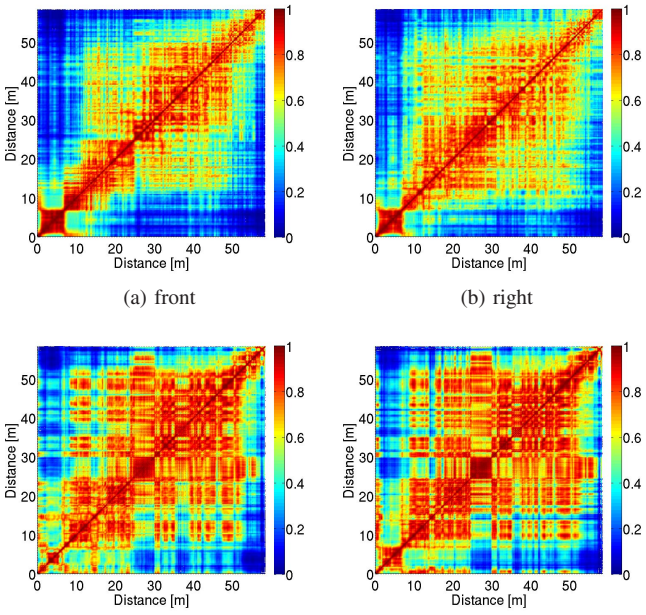

(a) front (b) right

(c) back (d) left

Fig. 2. Collinearity of the GLSF $col_{\mathbf{C}_{\mathrm{H}}^{(\Phi)}}$ for track 9a-9b

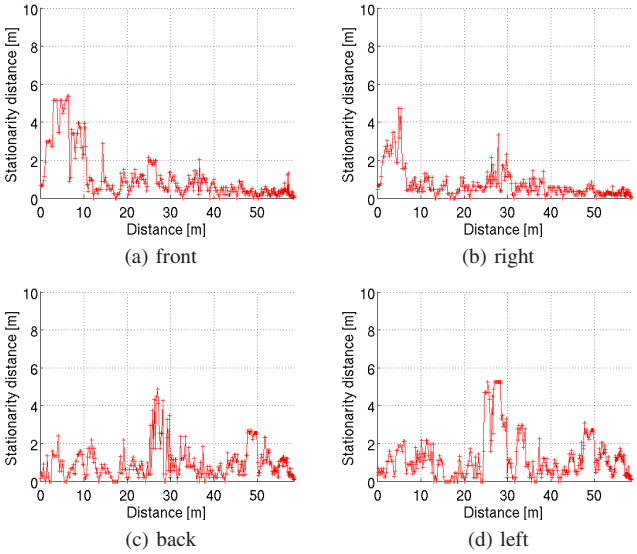

(a) front (b) right

(c) back (d) left

Fig. 3. Stationarity distances using $col_{\mathbf{C}_{\mathrm{H}}^{(\Phi)}}$ for track 9a-9b

just before the MT moves out of the open area. Table II shows the average stationarity distances $d_{stat,avg}$ per orientation for each track. They are rather short and range between 0.23 m and 2.75 m. Longer average stationarity distances are observed where main reflections are located: for track 10b-9a a line of sight (LOS) component is expected to occur partly for the back and the left orientation, and for track 41a-42 a strong constant reflection is expected for the front and right orientation due to a high building located close by. This could explain the slightly larger $d_{stat,avg}$ for these orientations.

Regarding the stationarity of the spatial properties only, Fig. 4 examplarily displays the full, TX, and RX CMD for the beginning of track 9a-9b and the front orientation. The full CMD shows larger values compared to the TX and RX CMD, since it considers variation in the spatial domain at the TX and the RX. The RX CMD is mostly lower than the TX CMD. Fig. 5 shows the resulting evolution of the stationarity distances for the whole track. The stationarity distance for the TX CMD rises after ca. 13 m. This behaviour is expected, since the BS (TX) is fixed and located at 25 m height. We, thus, expect less significant changes in the surroundings of the BS. Table III gives the average stationarity distances $d_{stat,avg}$ per orientation for each track and each CMD. We observe a strong variation: $d_{stat,avg}$ can vary from 0.97 m to the whole track length. Here, we cannot confirm a dependency of the average stationarity distances on the potential existence of a main reflection. However, $d_{stat,avg}$ can vary strongly with the MT orientation, especially for the TX CMD, cf. Table III.

The stationarity in distance of the time-frequency properties seems to be significantly shorter than the one of the spa-

Track	$d_{stat,avg}$ per orientation [m]			
	front	right	back	left
10b-9a	1.80	1.34	2.20	2.75
9a-9b	0.96	0.64	0.93	1.21
41a-42	0.80	1.41	0.23	0.42

TABLE II
Average stationarity distances using $col_{\mathbf{C}_{\mathrm{H}}^{(\Phi)}}$

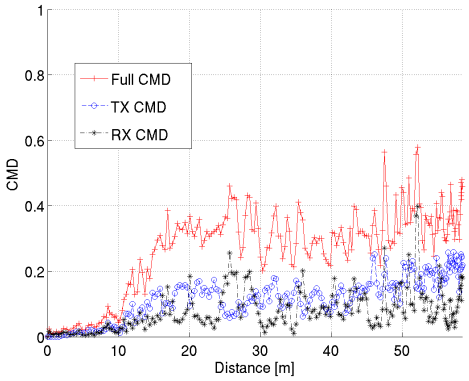

Fig. 4. CMDs for the beginning of track 9a-9b (front orientation)

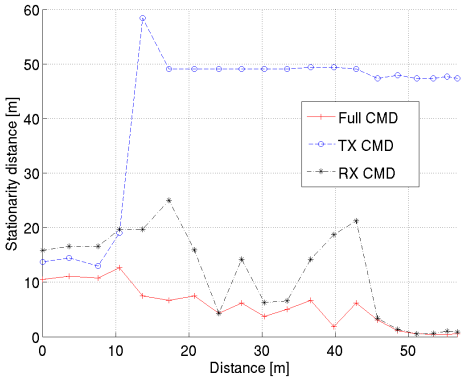

Fig. 5. Stationarity distances using the CMDs (track 9a-9b, front orientation)

tial properties, even when considering both spatial domains jointly, i.e., the full CMD, cf. Table II and Table III. Thus, we deduce that the time-frequency properties are dominant in defining stationarity regions. This observation is obviously bound to our specific scenario and site, e.g., to the time, frequency, and space parameters as well as to the chosen measure. Note also that the Doppler resolution of the GLSF depends on the length of the windows in time. Moreover, there is no apparent similarity in the stationarity distances of the orientations parallel to the street, i.e., the front and the back orientation (street canyon behavior). The same is true for the orientations perpendicular to the street, i.e., the right and the left orientation (large scatterer obstruction); here a reason can be the asymmetry due to driving on the right side of the street.

We expect that the stationarity in distance is dependend on the used array structures and antenna patterns. More generally, one can say that the array structures and the antennas are considered to be a part of the channel.

CMD	Track	$d_{stat,avg}$ per orientation [m]			
		front	right	back	left
full	10b-9a	6.12	3.00	3.51	5.36
	9a-9b	5.34	4.46	1.79	2.35
	41a-42	1.93	5.73	0.97	2.53
TX	10b-9a	31.24	16.66	20.56	12.58
	9a-9b	42.29	43.19	10.22	16.63
	41a-42	52.61	53.66	34.11	35.47
RX	10b-9a	12.81	4.85	5.13	12.48
	9a-9b	11.12	12.16	22.53	15.04
	41a-42	2.47	7.09	2.25	4.17

TABLE III
AVERAGE STATIONARITY DISTANCES USING THE CMDS

VII. Conclusion

We characterized the non-stationarity of the wireless channel in an urban macrocell scenario. Based on the collinearity measure, we determined quasi-stationarity regions in distance using second order moments only. In particular, we studied the dependence of these quasi-stationarity regions on the MT orientation. The time-frequency properties seem to be influenced by the appearance of LOS components or strong constant reflections, i.e., longer quasi-stationarity distances are observed in these cases. The quasi-stationarity of the spatial properties, especially at the BS, shows a strong dependence on the MT orientation. Moreover, the spatial properties at the BS are mostly slowly changing, meaning that, e.g., beamforming applications using the BS correlation matrix do not require frequent updates. The comparison of the quasi-stationarity in distance of the time-frequency properties to the one of the spatial properties showed that the time-frequency properties are, based on the chosen measure and in our specific scenario, dominant in defining the size of quasi-stationarity regions. We emphasize that the selection of an appropriate threshold for the measures depends on the accuracy required for the considered algorithm. A parametric estimation of the channel as well as a distinction between LOS and non-LOS scenarios is not considered here, but is left to a future work.

References

[1] L. Dossi et al., "Statistical analysis of measured impulse response functions of 2.0 GHz indoor radio channels," *IEEE J. Sel. Areas Commun.*, vol. 14, no. 3, pp. 405–410, Apr. 1996.

[2] A. Gehring et al., "Empirical channel stationarity in urban environments," in *Proc. of the 4th European Personal Mobile Communications Conference, Vienna, Austria*, Feb. 2001.

[3] P. Bello, "Characterization of randomly time-variant linear channels," *IEEE Trans. Commun. Syst.*, vol. 11, no. 4, pp. 360–393, Dec. 1963.

[4] G. Matz, "On non-WSSUS wireless fading channels," *IEEE Trans. Wireless Commun.*, vol. 4, no. 5, pp. 2465–2478, Sep. 2005.

[5] ——, "Doubly underspread non-WSSUS channels: Analysis and estimation of channel statistics," in *4th IEEE Workshop on Signal Processing Advances in Wireless Commun.*, Jun. 2003, pp. 190–194.

[6] A. Paier et al., "Non-WSSUS vehicular channel characterization in highway and urban scenarios at 5.2 GHz using the local scattering function," in *Int. ITG Workshop on Smart Antennas, Darmstadt, Germany*, Feb. 2008.

[7] L. Bernadó et al., "Non-WSSUS vehicular channel characterization at 5.2 GHz - spectral divergence and time-variant coherence parameters," in *Proc. of the XXIXth URSI General Assembly, Chicago, USA*, Aug. 2008.

[8] M. Herdin et al., "A MIMO correlation matrix based metric for characterizing non-stationarity," in *Proc. of the IST Mobile and Wireless Communications Summit, Lyon, France*, Jun. 2004.

[9] M. Herdin, "Non-stationary indoor MIMO radio channels," Ph.D. dissertation, Vienna University of Technology, Vienna, Austria, 2004.

[10] W. Kozek et al., "Quadratic time-varying spectral estimation for underspread processes," in *IEEE-SP Int. Symposium on Time-Frequency and Time-Scale Analysis*, Oct. 1994, pp. 460–463.

[11] C. Schneider et al., "Multi-user MIMO channel reference data for channel modelling and system evaluation from measurements," in *Int. ITG Workshop on Smart Antennas, Berlin, Germany*, Feb. 2009.

[12] MEDAV GmbH. (2009) Channelsounder properties. [Online]. Available: http://www.channelsounder.de

[13] IST-4-027756 WINNER II D1.1.2 V1.2. (2008, Feb.) WINNER II channel models. [Online]. Available: http://www.ist-winner.org

[14] D. Slepian, "Prolate spheroidal wave functions, Fourier analysis, and uncertainty - V: The discrete case," *Bell System Technical Journal*, vol. 57, pp. 1371–1430, Jun 1978.